Detection and quantification of bar breakage harmonics evolutions in inverter-fed motors through the dragon transform.

Vanessa Fernandez-Cavero[a], Joan Pons-Llinares[b,*], Oscar Duque-Perez[a], Daniel Morinigo-Sotelo[a]

[a] *Research Group ADIRE, Department of Electrical Engineering, University of Valladolid, Paseo del Cauce 59, 47011 Valladolid, Spain.*

[b] *Instituto de Ingeniería Energética, Universitat Politècnica de València, Camí de Vera s/n, 46022, València, Spain.*

* Corresponding author: J. Pons-Llinares, jpons@die.upv.es, Tel: 0034 963879599, Fax: 0034 963877429.

ABSTRACT: The paper shows that, the harmonics at the inverter output voltage grow the rotor solicitations of the induction motor fed, due to an increase of the temperature, harmonic torques created, and the higher chances of cage vibration resonances. Therefore, bar breakages appear under overloads, regenerative breaking stresses, or duty cycles with multiple steady state speeds and startups. Nonetheless, the bar breakage components, which evolve very close to the fundamental in inverter-fed motors, can only be detected if the fundamental component is represented as a very thin line, reducing the spread of its big energy. The problem of detecting and quantifying the bar breakage harmonics has not been solved by the time-frequency transforms present in the technical literature. The paper optimizes the use of atom-based time-frequency transforms, showing that with rectangular shapes atoms, only the steady state evolutions of the bar breakage components are obtained, and with inclined linear shapes, the bar breakage components are detected only during a part of the startup. Therefore, the dragon transform is introduced to solve the problem. The dragon atoms are defined with shapes perfectly adapted to the harmonics evolutions, no matter how

complex they are. As a consequence, the dragon transform enables to precisely trace in the time-frequency plane, the complete evolutions of the harmonics to be detected. A quantification method is proposed, which obtains for the first time in the technical literature, the time evolutions of the harmonics amplitudes, during a complex transient as the startup and the steady state of an inverter-fed motor. The transform performance is validated, testing the induction motor under different load levels.

Key words: Time-frequency analysis, transient analysis, ~~wavelet transform~~, ~~chirplet, signal analysis~~, fault diagnosis, rotor broken bar, induction motors, ~~monitoring~~, ~~frequency converter~~, inverter.

1. Introduction.

The majority of the induction motors nowadays are inverter-fed. First, in fixed speed drives, the inverter enables to adapt the speed to the load requirements, reducing the power consumption [1]: 25% reduction when running at half speed [2]. Second, in variable speed drives, the inverter is mandatory. Among other drawbacks, directly feeding a motor highly increases the stress during startups, causing faults as bar breakages. Nevertheless, even if startup currents are lower (they may reach twice the rated current), these stresses also appear in inverter-fed motors, especially when they work under overloads, and must perform regenerative braking, as in the case of cement or paper and pulp industries, or when the duty cycle contains frequent starts [3] and multiple steady state speeds, as in electric traction.

Furthermore, the inverter higher harmonic content at low frequencies increase the temperature [4] and creates harmonic torques [5], enabling cage vibration resonances [6] (mechanical resonance cage fatigue failures cover 10% of total failures [7]), and finally growing the rotor solicitations. Especially in electric traction, with high power inverters with lower switching frequencies, covering wide speed ranges, and dealing with regenerative breaking through bidirectional converters, the manufacturers are introducing design-based solutions to prevent bar breakages, as inclining two out of three bars in the junction with the short-circuit ring, to hinder its detachment [8].

Therefore, rotor problems arise in inverter-fed motors, which can lead to winding damage [9], especially under centrifugal forces at high speeds [6], when the bars are detached from the slots [10], or the whole short-circuit ring is detached, as in the inverter-fed induction motor shown in [8]. Moreover, while the design and manufacture of other parts of the machine has improved, the rotor has not changed, and its percentage of the whole induction motor faults has increased [11]. Certain manufacturers have come up with possible solutions to this type of problem: improving torsional stiffness (Siemens, [12]), replace short-circuit rings by flexible wires in the slots (Siemens, [13]) or use elements between bars to increase the stiffness and reduce the stress between the bar and the short-circuit rings (Ansaldobreda, [5]).

Academia has been focusing its efforts in developing methods of induction motor diagnosis based on current analysis, due to its advantages [8], even if vibration methods are more commonly used in industry [14]. Since the inverter-fed motors work under changing speeds, the frequencies in the current change over time, and time-frequency transforms must be used to perform the analysis [15,16]. Moreover, even under a long steady state capture, the harmonics are more easily confused in its spectrum than in a time-frequency map related to a transient, taking into account that the harmonic content and noise caused by the inverter may overlap or hide the faulty harmonics, whose amplitudes also depend on the Fundamental Component (FC) frequency and the control [17],[18],[19]. Unlike directly-fed motors, the FC frequency changes when the motor is fed by an inverter [20]. Moreover, the slip frequency remains low, making the bar breakage harmonics evolve parallel and very close to the FC [21,22]. This two aspects make the fault detection a challenge, whose solution is the purpose of this paper.

There are mainly two types of transforms that can be used to obtain the time-frequency evolution of the components present in a signal: the Wigner-Ville Distributions (WVD) and the atom-based transforms. Regarding the WVD, they are not useful to obtain the evolutions of bar breakage harmonics in inverter-fed induction motors: the cross terms introduced by this type of transform cannot be erased using a kernel when the evolutions of the components to be detected are too close to each other as in this case [23]. The Short

Time Fourier Transform (STFT), which is the simplest atom-based time-frequency transform, is not able to separately trace the evolutions of the FC and the bar breakage harmonics: the FC energy disperses and hides the faulty harmonics evolutions [23]. The wavelet transform, which has been used in several works to diagnose inverter-fed induction motors [22], [20], [24], [25], does not improve the STFT result regarding bar breakages, since the atoms used by this transform are adapted only for increasing frequencies following approximately a parabola. More advanced atom-based transforms, as the Adaptive Slope Transform (AST) [26], has been applied to detect eccentricities in inverter-fed induction motors [27], but as will be shown through the paper, when dealing with bar breakages under this type of supply, they only achieve to obtain the evolutions during the steady state. Finally, the last atom-based transform, the Chirplet Transform (CT) [28],[8], only enables to obtain the bar breakage harmonics evolutions during a certain part of an inverter-fed startup. Among other transforms, the Hilbert Huang Transform has been also applied to diagnose inverter-fed motors, but when dealing with the detection of bar breakages, their procedure cannot separate the faulty harmonics from the FC [23]. Finally, other transforms propose a non-uniform resampling [29], which enables to obtain the evolution of the bar breakage harmonics when plotted in a space-frequency map instead of a time-frequency map. Nevertheless, they do not allow quantification, making the diagnosis impossible.

Concluding, the time-frequency transforms present in the technical literature, do not enable to obtain the evolutions of the bar breakage harmonics during the startup of an inverter-fed motor, quantifying their energies to perform a diagnosis. Two approaches enable quantification, but only obtain a part of the evolutions (AST), (CT), while a third approach enables plotting the evolution in a space-frequency map, without possible quantification. This is the first paper in which the evolutions of the bar breakage harmonics, during an inverter-fed induction motor startup and steady state, are plotted with precision as very thin lines, enabling the quantification of their instantaneous amplitudes.

2. Time-frequency evolutions of the harmonics to be detected.

The objective of analyzing a current with a time-frequency transform is to obtain the time-frequency evolutions of the current components (also called harmonics, even if some authors reserve this term only for steady state). If the faulty components are present in the current, their evolutions will appear in the transform result, enabling to detect their presence and quantify their amplitudes, allowing for a diagnosis to be performed (analyse if their presence in the current is important enough to relate it to the presence of the fault in the motor). Therefore, the evolution has to be traced complete and with enough precision to define a reliable quantification method of the harmonics amplitude.

In order to study which type of transform has to be applied to obtain such a result, the first step is to analyse the "structure" of the current; i.e., which are the kind of evolutions that the transform applied has to be able to reflect in the time-frequency graph obtained. Let us analyse it through an example: the stator current of an inverter-fed induction motor has been captured during a startup and the subsequent steady state, under a bar breakage (Fig. 1(a)). The motor and inverter characteristics can be found in section 5.

The bar breakage harmonics frequencies can be obtained through the Fundamental Component (FC) frequency f_{FC} and the slip s, using:

$$f_{BBH} = \left|1 \pm 2s\right| f_{FC} \tag{1}$$

These can be rewritten in terms of the slip frequency sf_{FC}:

$$f_{BBH} = \left|f_{FC} \pm 2sf_{FC}\right| \tag{2}$$

The FC frequency can be obtained through the current captured using the method presented in [27]. The slip can be obtained through the motor speed, acquired using a sensorless speed method [30], or directly

using a sensor (if any installed), as in this case. The FC frequency, the slip and the slip frequency evolutions are shown in Figs. 2 (a), (b) and (c) respectively, for the bar breakage case.

It can be seen how the inverter keeps the slip frequency low, and approximately constant (between 1 and 3 Hz). Therefore, as it can be deduced from (2), the bar breakage harmonics frequency is equal to the FC frequency, plus or minus twice the slip frequency (which is constant). Then, the bar breakage harmonics evolve parallel to the FC, separated twice the slip frequency, towards higher or lower frequencies, depending on the sign used in (2). This is exactly what can be observed in Fig. 1 (d), where the FC frequency has been plotted (blue) together with the bar breakage harmonics evolutions (red).

It can be concluded that, in the case of an inverter-fed motor, the bar breakage harmonics evolve very close to the FC. Taking into account that the FC has a much higher energy than the faulty harmonics, the detection of these harmonics is very difficult. The challenge is to represent the FC evolution in the time-frequency plane as a very thin line: if its energy spreads around its real evolution, being represented as a line with a certain thickness, it will uncover the faulty harmonics evolutions.

3. Time-frequency atoms and resolution trade-off.

Time-frequency transforms try to obtain the time-frequency evolutions of the components in the signal analysed. Basically, there are two types of transforms: the Wigner-Ville distributions and the atom-based. The Wigner-Ville distributions are not considered here, since they introduce cross-terms, which are very difficult to be removed using kernels when the harmonic evolutions are so close to each other as in this case (see previous section). On the other hand, atom-based transforms generate clear results, without cross terms. Nevertheless, they have an inherent resolution trade-off which has to be solved.

Briefly, a time-frequency atom is a function whose energy is well concentrated around a point of the time-frequency plane. Figure 2 (a) shows the same evolutions of the FC and the bar breakage harmonics of

Fig. 1 (d), plotted in white. The time-frequency energy distribution of seven atoms has been represented too. The atoms are centred at different points along the Lower Sideband Harmonic evolution (LSH, bar breakage harmonic below the FC). The present paper uses Gabor atoms ϕ, defined by a Gaussian window g (3), with a time dispersion characterized by its deviation parameter σ, centred in t_c, normalized with a constant $C_\sigma = 1/\left(\sqrt[4]{\pi}\sqrt{\sigma}\right)$, and modulated at a frequency f_c:

$$g(t) = C_\sigma e^{-\frac{(t-t_c)^2}{2\sigma^2}} \quad \rightarrow \quad \phi(t) = g(t) e^{i2\pi f_c (t-t_c)} \tag{3}$$

Each atom's energy is confined in its respective enlarged Heisenberg box. This box, plotted in white in Fig. 2, describes how the energy of the atom disperses from its centre along the plane (see section 2 in [26] for a deep introduction). For instance, the five atoms centred along the startup have a box more or less squared, while the two atoms centred in points of the steady state have a flatter rectangular box, which describes the rectangular shape of their energy dispersion in the plane. The correlation between the atom and the signal to be analysed, measures the energy of the signal inside the atom's enlarged Heisenberg box; correlating is like multiplying the time-frequency energy distributions of the atom and the signal analysed: everything outside the atom's enlarged Heisenberg box is cancelled, and only the energy of the signal inside is measured. More precisely, it can be demonstrated that the square of the correlation is a measure of the signal's energy density inside the box. If the operation is repeated in several points of the time-frequency plane correlating with atoms centred in those points, the energy density along the plane will be obtained, showing how the energy of the signal is distributed. The energy density of the signal will be high in the points of the time-frequency plane with harmonics evolutions, and low everywhere else. Therefore, representing the energy density of the signal obtained through atoms correlations, gives as result the time-frequency evolutions of the harmonics contained in the signal analysed.

The question is: which is the best "shape" of the atom to be used? When using atoms with "rectangular" energy distributions (as the ones shown in Fig. 2), the best shape is obtained applying the slope criterion [26],[27]: if an atom is centred in a certain point of a harmonic evolution, to capture the energy of that harmonic at that point, the diagonal of its Heisenberg box must match the tangent to the harmonic evolution at that point. Since the LSH evolution along the startup is approximately rectilinear, the tangent at every of these evolution points is the LSH evolution itself. Therefore, the atoms used along the startup in Fig. 2 (a) have a Heisenberg box diagonal that matches the evolution of the LSH. The atoms in the steady state, since the tangent to the LSH evolution is a horizontal line, they should be completely flat. Nevertheless, this is not recommended since the atom energy would disperse form minus to plus infinity.

The problem is that the FC evolution crosses every of the five boxes of the atoms centred along the LSH evolution during the startup. Therefore, when correlating those atoms with the signal analysed, even if they try to measure only the LSH energy around the points where they are centred, the FC energy would be measured too, since the correlation measures the energy inside the box, and those boxes contain parts of the FC evolution. If a flatter box is used (Fig. 2 (b)), we are trying to avoid crossing the FC evolution in the upper part of the box, but a bigger part is captured at the left part of the box. Analogously, if a taller box is used (Fig. 2 (c)), the FC interacts less with the left part of the box, but crosses more in its upper part. The slope criterion has the best compromise, not only to capture the highest amount of the LSH energy [26], but also to avoid the FC.

Nevertheless, this is not enough. Figure 2 (d) shows atoms centred along the three evolutions, using the slope criterion. It can be observed that, since the three evolutions are nearly parallel along the startup, the tangents to these evolutions are also parallel. Moreover, since the evolutions are nearly rectilinear, their tangents nearly do not change along the startup. Therefore, all the atoms along the startup, with diagonals matching the tangents, have nearly the same shape. Therefore, in order to construct the final family of atoms

to be used to correlate with the signal, atoms with the same shapes are used along all the plane during the startup, changing to a flatter rectangular shape when the steady state arrives (Fig. 3, left). The result of the transform, called Adaptive Slope Transform (AST, used in [26] to detect bar breakages in directly-fed motors, and in [27] to detect eccentricities in inverter-fed motors), is shown in Fig. 3, right. As predicted, the atoms centred at the LSH evolution, capture the FC energy, which disperses till those points, hiding the LSH evolution. In other words, the energy of the FC spreads around its evolution, hiding the evolutions of the bar breakage components during the startup. Only during the steady state, an atom centred at the FC, only captures the FC energy, while an atom centred in the LSH, only captures the LSH energy. This is due to the fact that the atom's shape are truly adapted to the harmonics evolutions they are trying to detect, and they appear traced as thin lines, enabling to distinguish the three evolutions.

The atoms can change their shapes from the classic rectangular dispersion of their energy. In this type of atoms, as shown in (3), the window is modulated multiplying with a complex exponential of angle $\theta(t) = f_c(t - t_c)$ (expressed in degrees instead of radians). The derivative of that angle gives the frequency at which the window is modulated, which in this case it is constant:

$$\theta(t) = f_c(t - t_c) \quad \rightarrow \quad \frac{d\theta(t)}{dt} = f_c \tag{4}$$

Let us construct an atom with a flat rectangular dispersion of its energy (lower atom in Fig. 4, left). This is simply achieved by taking a high deviation parameter σ in (5): the atom's energy disperses in time. Then, in order to construct the upper atom in Fig. 4, left, instead of modulating the Gaussian window at a constant frequency f_c (as in (5)), the modulation is performed as follows:

$$g(t) = C_\sigma e^{-\frac{(t-t_c)^2}{2\sigma^2}} \quad \rightarrow \quad \phi(t) = g(t) e^{i2\pi\left(f_c(t-t_c)+\frac{S}{2}(t-t_c)^2\right)} \tag{5}$$

The instantaneous frequency in (6) increases linearly in time with a slope S being f_c when $t = t_c$:

$$\theta(t) = f_c(t - t_c) + \frac{S}{2}(t - t_c)^2 \quad \rightarrow \quad \frac{d\theta(t)}{dt} = f_c + S(t - t_c) \tag{6}$$

The slope S determines the "inclination" of the atom. If $S = 0$ Hz/s, then equations (4) and (6) are equal, and taking $f_c = 5$ Hz, the lower atom in Fig. 4, left, is obtained, which has none inclination. If $S = 2.5$ Hz/s, and taking $f_c = 12.5$ Hz, the upper atom is constructed: it has an energy dispersion that follows a straight line; the slope S fixes the inclination of the line that the energy dispersion is going to follow, while it's energy main centre frequency still being f_c. These atoms are called chirplets. The resulting transform is called Chirplet Transform (CT). In Figure 4, right, the same evolutions of the FC and the bar breakage harmonics of Fig. 1 (d) are plotted in white. Moreover, the energy distributions of five chirplet atoms have been represented. The chirplets have been chosen with a slope $S = 5$ Hz/s, equal to the slope of the LSH evolution during the startup (evolves from 0 to 50 Hz in 10 s). This way, their shape fits the evolution of the harmonic to be detected during the startup. They have been centred in three points of the startup and two points of the steady state. Since the FC and the other bar breakage harmonic evolve in parallel, the chirplets constructed with this slope would fit also their evolutions during the startup when centred to capture them.

Figure 5 shows a whole family of chirplets distributed along the time-frequency plane, together with the evolutions of the FC and the bar breakage harmonics to be detected. One of the drawbacks of the CT is that the inclination of the chirplets must be the same for every point of the plane analysed. The chirplets are chosen with a 5 Hz/s slope, adequate to match the evolutions of the three harmonics during the startup. The result of the CT is shown in Fig. 7, right. It can be observed that the FC evolution appears as a very thin line during a certain part of the startup. Same thing happens with the bar breakage components. In this region, their evolutions can be distinguished very well. Nevertheless, a chirplet centred with this shape around a

point of the FC steady state, captures its energy, unless it is centred far away from its evolution. Therefore, the FC energy spreads widely around its evolution, masking the end of the startup, and everything around the steady state, and particularly hiding the evolutions of the bar breakage harmonics.

In the present section, the best results have been obtained when using atoms with rectangular shapes (AST), and when using atoms with inclined linear shapes (CT). As seen through the results presented, these time-frequency transforms do not enable to obtain the evolutions of the bar breakage harmonics during the startup of an inverter-fed motor. This is due to the fact that, in this case, the faulty harmonics evolutions are too close to the FC. To prevent the FC from hiding the faulty harmonics, its evolution has to be plotted as a thin line. Nevertheless, this only happens during the steady state for the AST, and during a part of the startup for the CT. Therefore, the AST only achieves to detect the bar breakage harmonics evolutions during the steady state, and the CT only during a part of the startup. None of them enables to plot the whole evolution of the faulty harmonics. For this reason, a new transform is defined in the following section, using a new type of atom.

4. Dragon transform.

As seen in the previous sections, the main problem to detect the FC and the bar breakage evolutions in an inverter-fed induction motor startup, is that they are too close to each other. To distinguish them in the time-frequency plane, the transform must be able to trace them as very thin lines. This is achieved when the energy dispersion of the atom used follows the evolution of the component to be detected. Then, the energy dispersion of the component itself, when represented in the time-frequency map, takes place also along its own evolution. As a result, the component evolution is traced as a very thin line, without nearly any thickness. In the present section, the dragon atoms (which have the mentioned characteristics) are defined and build. Then, the dragon transform, based on the use of dragon atoms, is also defined and applied. Finally, a quantification method is introduced to obtain the instantaneous amplitudes of the harmonics detected.

4.1. Building atoms following arbitrary evolutions.

The dragon atoms are defined as atoms whose energy disperses following the evolution of the component to be detected. In other words, the shape of the atom fits the evolution of the component. To achieve this, the modulation must be performed differently at each time instant. More precisely, the window must be modulated using an angle $\theta(t)$ in the complex exponential (7), whose time derivative is equal to the time evolution of the component's frequency $f(t)$:

$$g(t) = C_\sigma e^{-\frac{(t-t_c)^2}{2\sigma^2}} \quad \rightarrow \quad \phi(t) = g(t) e^{i\theta(t)} \quad \rightarrow \quad \frac{d\theta(t)}{dt} = f(t) \tag{7}$$

Figure 6 shows, at the left, the time evolutions of the frequencies from two monocomponent synthetic signals. The first monocomponent signal has a decreasing frequency changing to a horizontal evolution (up), while the second describes a sinusoidal time evolutions (down). The right part of the figure, shows the energy distributions of four (up) and five (down) dragon atoms centered in different points and defined to fit the evolutions of the monocomponent signals in the left part of the figure. As it can be observed, the atoms follow the time-frequency evolutions of the synthetic signals, not only during their rectilinear periods, but also during the points of change, as at 10 s. In the second signal (down) the energy distributions of five dragon atoms have been represented in the right part of the figure, showing how precisely the dragon atoms follow the evolutions of the components to be detected.

The dragon atoms that have been defined and built in the present section of the paper, are able to adapt to the shape of a harmonic time evolution, no matter how its frequency changes in time. As it will be shown in the next subsection, this will enable to plot the harmonic evolution as a very thin line. This is due to the fact that, when using a dragon atom, the energy dispersion happens along the harmonic evolution itself.

4.2. Transform definition.

The dragon transform is defined as the correlation between the signal to be analyzed h with a family of dragon atoms ϕ:

$$\langle h,\phi\rangle = \int_{-\infty}^{+\infty} h(t)\phi^*(t)dt = \int_{-\infty}^{+\infty} h(t)C_\sigma e^{-\frac{(t-t_c)^2}{2\sigma^2}} e^{-i\theta(t)}dt \quad \rightarrow \quad \frac{d\theta(t)}{dt} = f(t) \tag{8}$$

The key point is to properly define the family of dragon atoms. To start with, t_c is the time instant where the atom is centred (fixed when the time instant analysed by the atom is chosen). As previously mentioned when explaining Fig. 4, left, the deviation parameter σ is taken high enough to obtain a thin atom (the constant that normalizes is automatically defined $C_\sigma = 1/\left(\sqrt[4]{\pi}\sqrt{\sigma}\right)$). The only magnitude remaining in (8) to perform the calculation is the most important one: the angle in the complex exponential.

Basically, two possible situations must be considered: an atom centered in a point where a component of the signal evolves, and an atom centered in a point where no component of the signal evolves. In the case of the signal analyzed (the startup current of an inverter-fed induction motor), there are three components whose evolutions must be properly traced to diagnose the rotor state: the FC and the bar breakage harmonics (plotted in blue and red respectively in Fig. 7, left). For this first case, in which the atom is centered in one of these three evolutions, the atom must simply fit the evolution to be detected. To achieve this, the time evolution of the component's frequency must be obtained, taking $k=0$ for the FC, $k=1$ for the Upper Sideband Harmonic (USH), and $k=-1$ for the LSH in the following equation:

$$\frac{d\theta(t)}{dt} = f(t) = \left|1+2ks(t)\right| f_{FC}(t) \tag{9}$$

Once the derivative of the angle is determined, numerical integration is applied (taking a zero initial value, since it has no effect on the result of the transform), and the resulting angle is used in (8) to obtain the correlation. Figure 7, right, shows the energy distributions of fifteen dragon atoms, centered at several points of the FC, LSH and USH evolutions, defined following this procedure.

Let us approach the second situation: atoms centered in points where no evolution appears. The procedure is to define an evolution crossing that point and parallel to the FC, LSH and USH evolutions, and then, define the atom to fit that evolution. If we give positive values to $k \in \mathbb{Z}$,(9) describes evolutions parallel to the USH evolution tending to higher frequencies. If on the contrary, negative values are assigned to $k \in \mathbb{Z}$, the equation describes evolutions parallel to the LSH towards zero. Generally speaking, if instead of taking $k \in \mathbb{Z}$, we take $k \in \mathbb{R}$, a whole family of parallel evolutions appear in the time-frequency plane (in which the FC, LSH and USH evolutions are included when $k=0$, $k=-1$ and $k=1$ are taken respectively). All this evolutions are parallel: they do not cross each other. Therefore, for each point of the time-frequency plane (t_c, f_c), there exists only one evolution crossing that point. The value of $k \in \mathbb{R}$ which defines the evolution crossing (t_c, f_c) is given by:

$$k(t_c, f_c) = \frac{1}{2s(t_c)}\left[\frac{f_c}{f_{FC}(t_c)} - 1\right] \tag{10}$$

If an atom is centered in (t_c, f_c), the value of $k(t_c, f_c)$ which defines the evolution crossing (t_c, f_c) is obtained using (10). Then, the evolution itself is obtained using (11): $f(t) = \left|1 + 2k(t_c, f_c)s(t)\right| f_{FC}(t)$. Then, that frequency time evolution is numerically integrated to obtain the angle finally applied in (8).

To conclude, the only difference between the procedure when using an atom that is centred in the FC, LSH or USH evolutions, and an atom centred anywhere else, is that for the first case $k=0$, $k=-1$ and $k=1$ are taken respectively, and for all the other cases k is calculated using (10). In fact, if a point of the plane contained in the evolutions of FC, LSH or USH is considered, and the value of k is calculated through (10), it will give as a result $k=0$, $k=-1$ and $k=1$. Therefore, exactly the same procedure can be applied for every point of the time-frequency plane analysed.

If we apply this procedure to the current analyzed, the family of dragon atoms shown in Fig. 8 is constructed. We can see that the further we move from the FC evolution, a bigger "ripple" appears in the energy dispersion of the atoms. This is caused by an inherent ripple in the speed measured, which is transferred to the slip, and finally to the frequencies time evolutions obtained through (11), which have to be followed by the dragon atoms. Since in (9) k multiplies the slip, the ripple in the frequencies calculated through (9) will get higher for higher $|k|$, and $|k|$ increases when moving far from the FC evolution ($k=0$ along the FC evolution). As it can be seen in Fig. 8, the dragon atoms even achieve to follow those ripples of the frequency time evolutions obtained through (9). The result from correlating the signal with the family of dragon atoms, obtaining the dragon transform result, is shown in Fig. 8, right. Several zooms of this result can be seen in Fig. 9.

As it has been shown through the results, the dragon atoms perfectly adapt to the evolutions of the FC (Fig. 7, right), and the bar breakage harmonics, not only during the startup, but also during the steady state. Moreover, it has been constructed a smooth family of dragon atoms (Fig. 8, left), whose shapes change uniformly from one to the next, following evolutions that do not cross. As a result, the evolutions of the FC, LSH and USH are represented very precisely in the time-frequency plane as perfectly traced thin lines (Fig. 8, right). Even if their evolutions are very close, due to the lack of thickness when plotted in the time-frequency plane, they can be distinguished along the complete transient captured (startup and steady state).

Particularly, in Fig. 9, the evolutions at the beginning, the middle and the end of the startup can be separately observed, being able to follow their frequency change when the steady state arrives, and finally describing horizontal evolutions. To conclude, the dragon transform enables, not only a very easy visual detection of the components evolutions when zooming, but it also enables to propose a quantification method to obtain its instantaneous amplitudes, and perform a reliable diagnosis, as shown in the next subsection.

4.3. Quantification method.

The quantification method presented enables to obtain the time evolution of the harmonics amplitudes through the whole capture: the startup and its transition to the steady state. To achieve this goal, the dragon transform result is plotted in 3D, from two different perspectives (Fig. 10). In Fig. 11, left, the same result as in Fig. 10, left, is represented, but including three arrows showing the evolutions of the bar breakage harmonics: two for the LSH and one for the USH. Then, a frequency band is calculated around the LSH evolution obtained through (11) (FC and speed evolutions captured as explained in Section 2). That frequency band is represented in blue in Fig. 11, right. The width of the band is lower for the beginning of the startup and the change to the steady state, where more precision is needed. For each time instant, all the dragon transform results at that time and inside the blue frequency band are considered, obtaining its maximum. That maximum indicates the presence of the LSH evolution, plotted in red (Fig 11, right). Same procedure is applied to the USH, plotting the frequency band in green. The LSH and USH evolutions (red, Fig. 11, right), are finally superimposed in blue to the 3D result shown in Fig. 12, left. This enables to obtain, for each time instant, the instantaneous amplitude (in dB with respect to the FC amplitude), of the LSH and USH. These instantaneous amplitudes are finally plotted in Fig. 12, right, in blue and green respectively.

To conclude, this is the first paper which shows the evolutions, and quantifies also its amplitudes, of the bar breakage components, during a complex transient as the startup and the following steady state of an inverter-fed motor. Moreover, the evolutions are obtained complete, and with high precision, thanks to the dragon transform here defined.

5. Experimental results.

In order to prove the great capabilities of the dragon transform, experimental tests have been performed in a laboratory. The induction motor tested (Siemens) has a 1.1 kW rated power, and 1410 rpm rated speed. The motor has been connected in star, being the rated line voltage and current 400 V and 2.6 A respectively. A hole has been drilled in the rotor cage, to cause the bar breakage. The frequency converter used to feed the motor is an Allen Bradley PowerFlex 40 inverter. The inverter has been programmed to startup the motor in 10 s, through a FC frequency increasing linearly in time, starting at 0 and reaching 50 Hz in steady state (as seen in blue, in Fig. 13 top, for the two load levels used, low at the left and high at the right). An electromagnetic powder brake (Lucas Nülle) has been used as the motor load. To acquire the stator motor currents (at a sampling frequency of 5 kHz), a Hall effect sensor (LEM) is used, connected to an acquisition board (cDAQ-9174, National Instruments), USB controlled through a PC.

The motor has been tested under two load levels. First level is characterized by a 2.6 Nm resistance torque, at which the motor reaches the 51 % of its rated load. Second level is achieved through a 3.8 Nm resistance torque, which increases the load to a 74 %. The methodology presented in the paper has been applied in both cases, whose results are shown in Fig. 13: low load at the left, and high load at the right. At the top of Fig. 13, the evolutions of the FC (blue) and the bar breakage harmonics (red), can be seen. The FC evolution has been obtained through the stator current captured, applying the method presented in [27]. To plot the bar breakage harmonics evolutions, the time evolution of the slip must be obtained previously too. The control unit of the electromagnetic powder brake measures speed and torque. This speed measure has

been used to obtain the slip. The dragon transform has been applied as explained in the previous sections, showing the results at the middle of Fig. 13 (left for low load, right for high load). The quantification result is the time evolution of the energy density along the evolutions of the bar breakage harmonics, which are shown at the bottom part of Fig. 13.

As shown in the present section, the dragon transform works well in both low and high load conditions. The differences observed are only related on how close the harmonics evolutions are to the FC. The low load condition is the most challenging, since the evolutions are closer for this case (that's why this case has been chosen as the example to show, along the paper, how the dragon transform works). The quantification results obtained are very similar for both cases: the bar breakage harmonics amplitudes do not vary significantly with the load, for an induction motor started up through an inverter. It can be concluded that, the dragon transform enables to detect the bar breakage harmonics, even when they evolve really close to the FC due to low load, precisely showing its evolution along the inverter-fed startup, and obtaining the energy density time evolution of the faulty harmonics to quantify the rotor fault.

6. Conclusions.

As introduced in the abstract, and further explained through the paper, the high harmonic content of the inverter stimulates bar breakages in the induction motor, due to the temperature increase, harmonic torques generated, the increased chances of mechanical resonances and the final grown in rotor solicitations, especially in applications with overloads, regenerative breaking or with several startups and change of steady state speeds. Nevertheless, the detection of the bar breakage components evolutions is very difficult due to its vicinity to the FC. The paper presents an optimization of the atom-based transforms present in the technical literature: the FC evolution is only traced as a thin line during the steady state (rectangular atoms) or during a part of the startup (inclined atoms), spreading the high energy of the fundamental, and hiding the evolutions of the bar breakage components, in all the other parts of the transient.

To tackle this unsolved problem in the technical literature, the paper presents a new transform in which the dragon atoms are defined and build, perfectly adapting their shapes to the evolutions to be detected, no matter how complex the frequency time evolution might be. As a result, the dragon transform generates a time-frequency plot in which the evolutions of the FC and the bar breakage harmonics are traced as very thin lines during the whole capture. This enables a very precise and complete detection of the faulty harmonics evolutions. Moreover, the paper presents a quantification method which obtains the time evolution of the bar breakage harmonics amplitudes, enabling the diagnosis. The method has proven its capabilities under two different load levels, showing its excellent performance even under low load, when the faulty harmonics evolve really close to the fundamental. It can be concluded that the dragon transform is the first transform which enables a complete and very precise detection and amplitude quantification of the bar breakage harmonics evolutions during a complex transient as the whole startup and steady state of an inverter-fed induction motor.

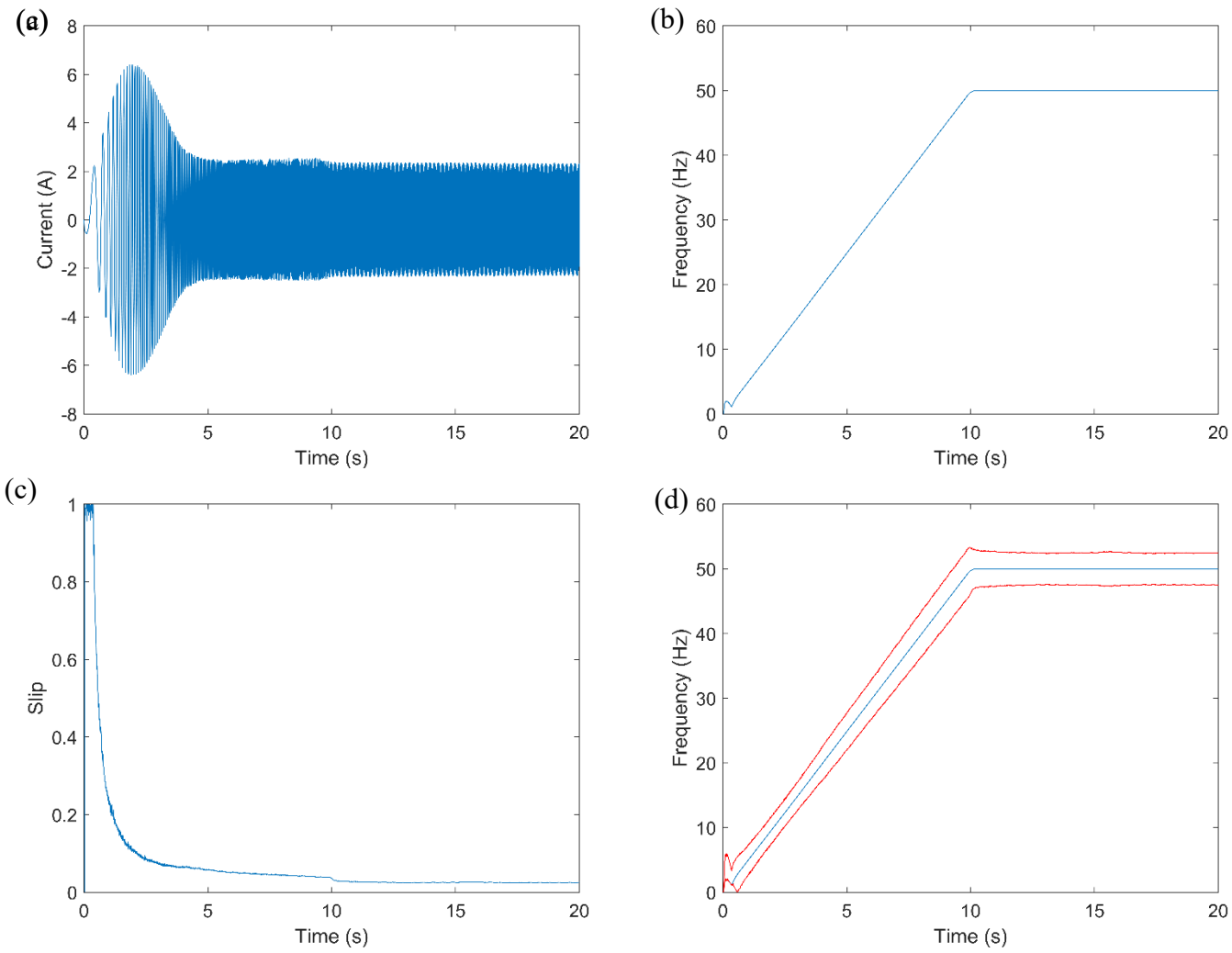

Fig. 1. Time evolution of the following magnitudes, during the startup and subsequent steady state of the induction motor with a bar breakage: Stator current (a), FC (b), slip (c) and FC in blue together with bar breakage components in red (d).

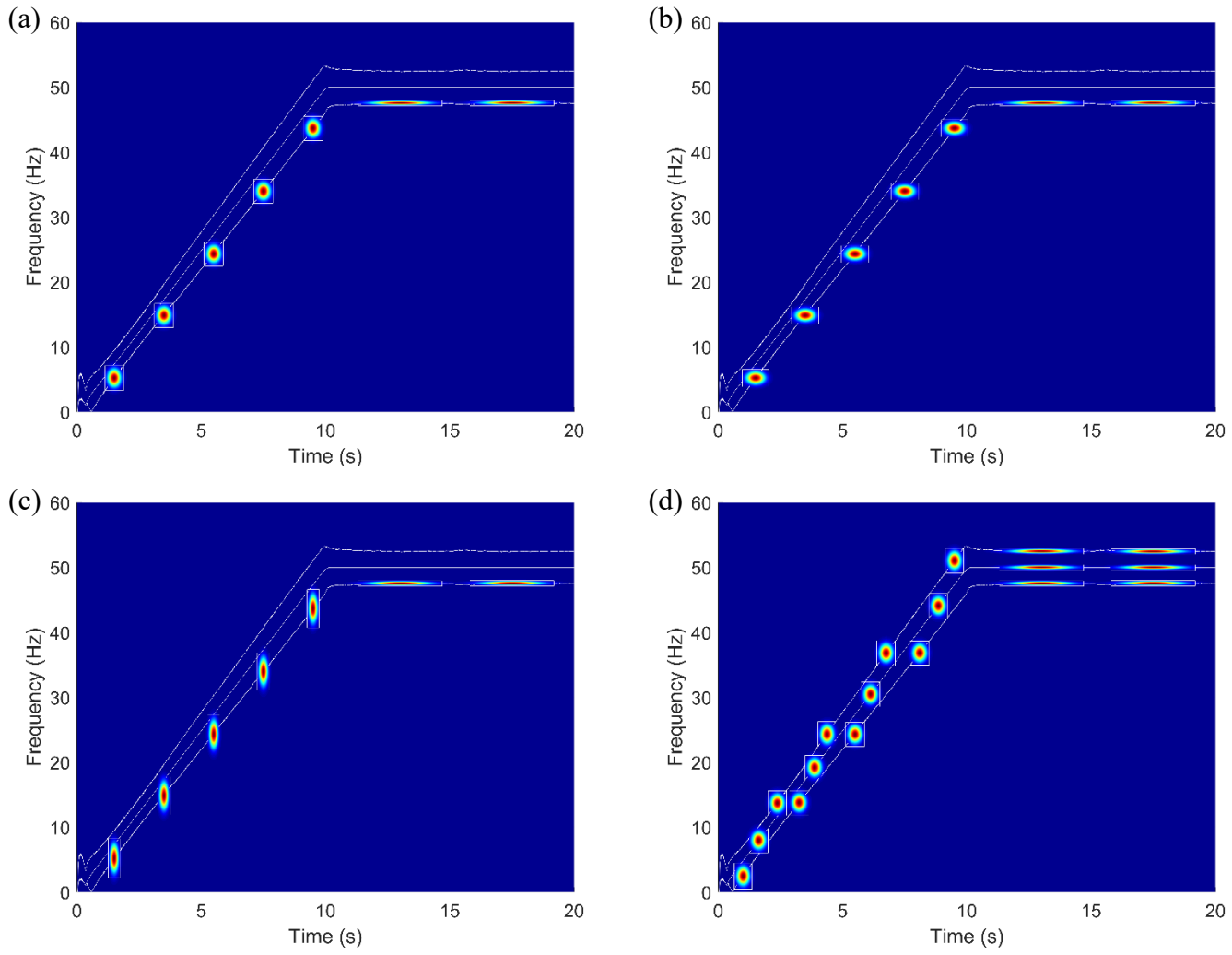

Fig. 2. Time-frequency evolutions of the FC and the bar breakage harmonics (white) together with the energy distribution of several time-frequency atoms along the lower sideband harmonic evolution, following the slope criterion (a), with a lower slope (b) with a higher slope (c) and distributed along the three evolutions, according with the slope criterion (d).

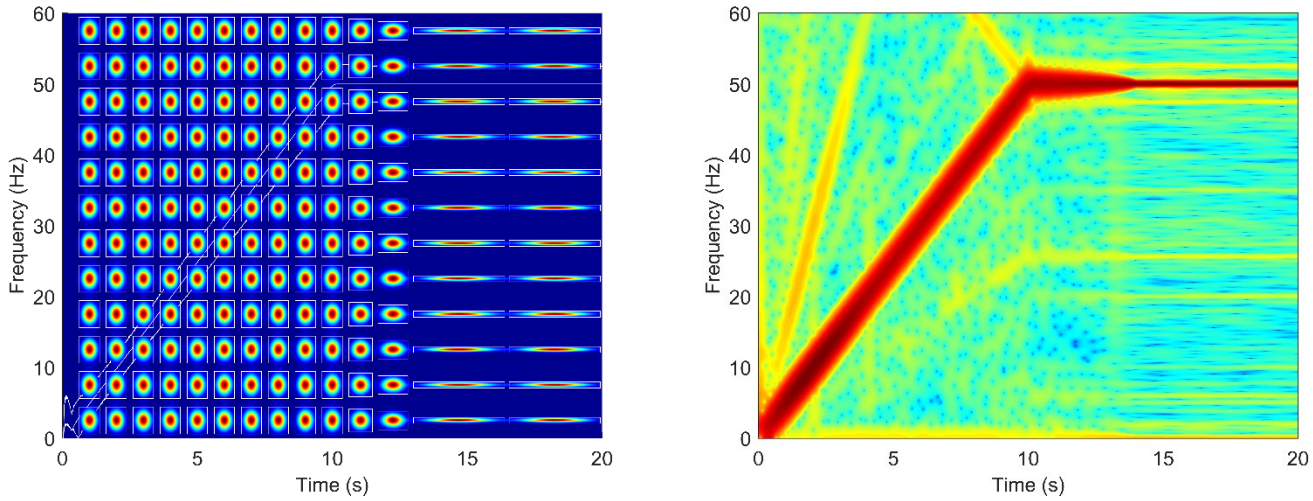

Fig. 3. Time-frequency evolutions of the FC and the bar breakage harmonics (white) together with the family of time-frequency atoms fixed with the slope criterion (left) and the resulting analysis (right) of the current from the bar breakage motor (AST).

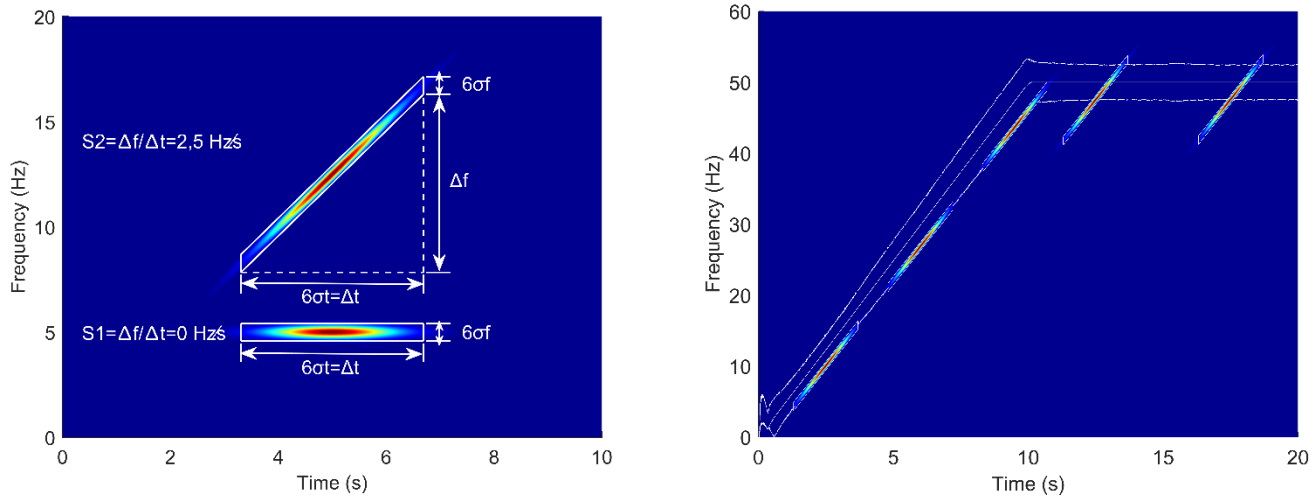

Fig. 4. Constructing a chirplet type of atom: energy distribution of chirplet atoms with 0 and 2.5 Hz/s slopes (left). Time-frequency evolutions of the FC and the bar breakage harmonics (white) together with the energy distribution of several chirplet type of atoms along the lower sideband harmonic evolution, adapted to that harmonic slope during the startup (right).

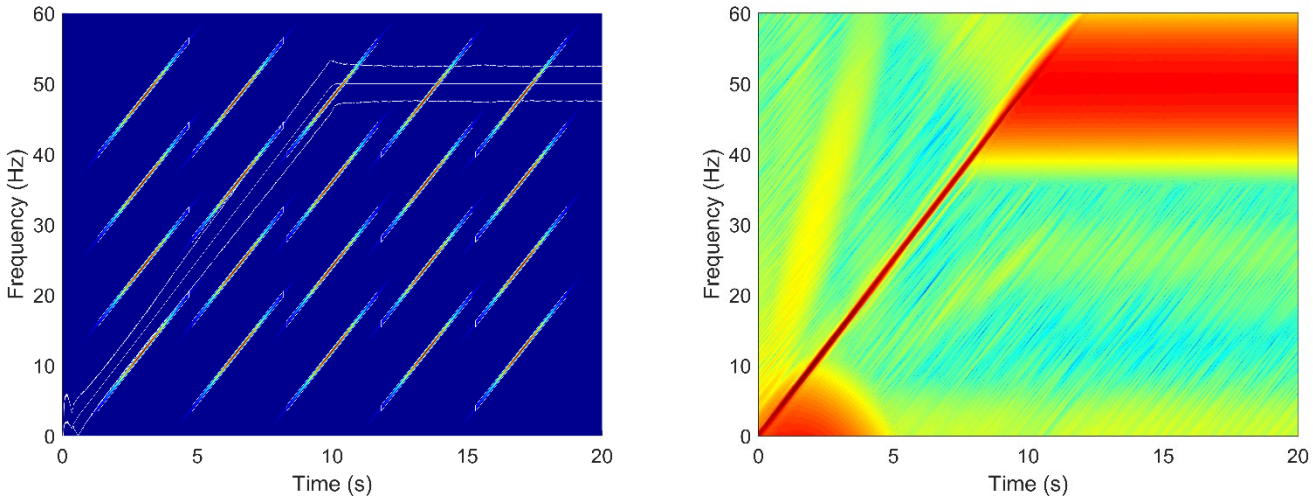

Fig. 5. Time-frequency evolutions of the FC and the bar breakage harmonics (white) together with the family of chirplet atoms adapted to the FC slope during the startup (left) and the resulting analysis (right) of the current from the bar breakage motor (CT).

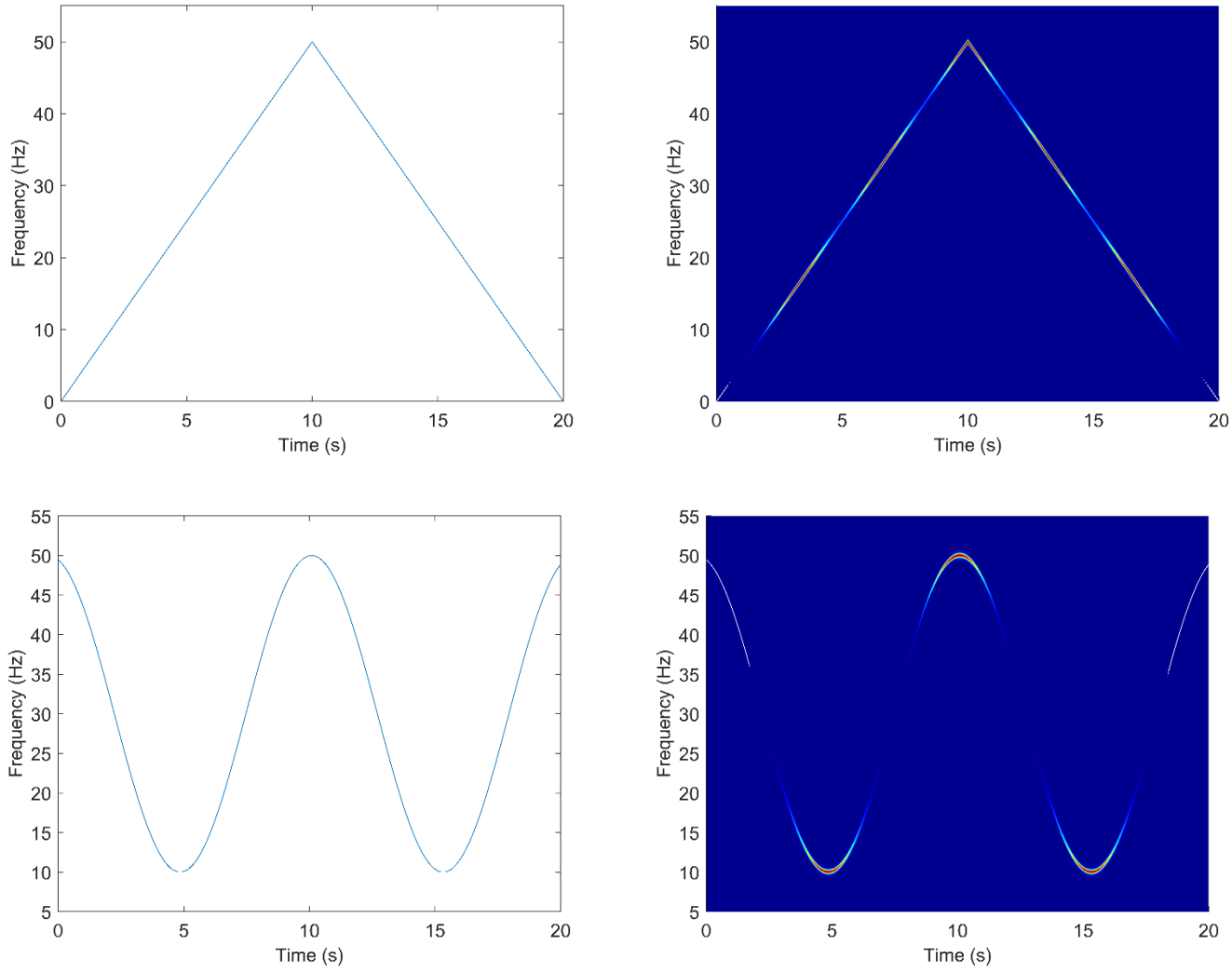

Fig. 6. Time-frequency evolutions of monocomponent synthetic signals (left), energy distribution of dragon atoms following these evolutions (right), for a triangular evolution (up) and for sinusoidal frequencies pulsating around 30 Hz (down).

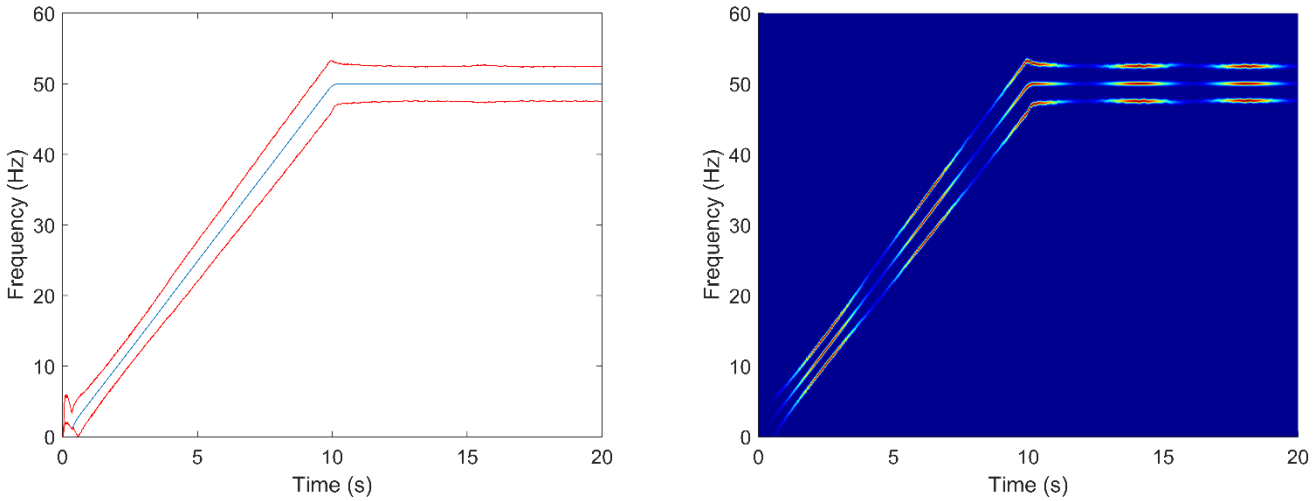

Fig. 7. Time-frequency evolutions (left) of the FC (blue) and the bar breakage harmonics (red), energy distributions of several dragon atoms along the three evolutions (right).

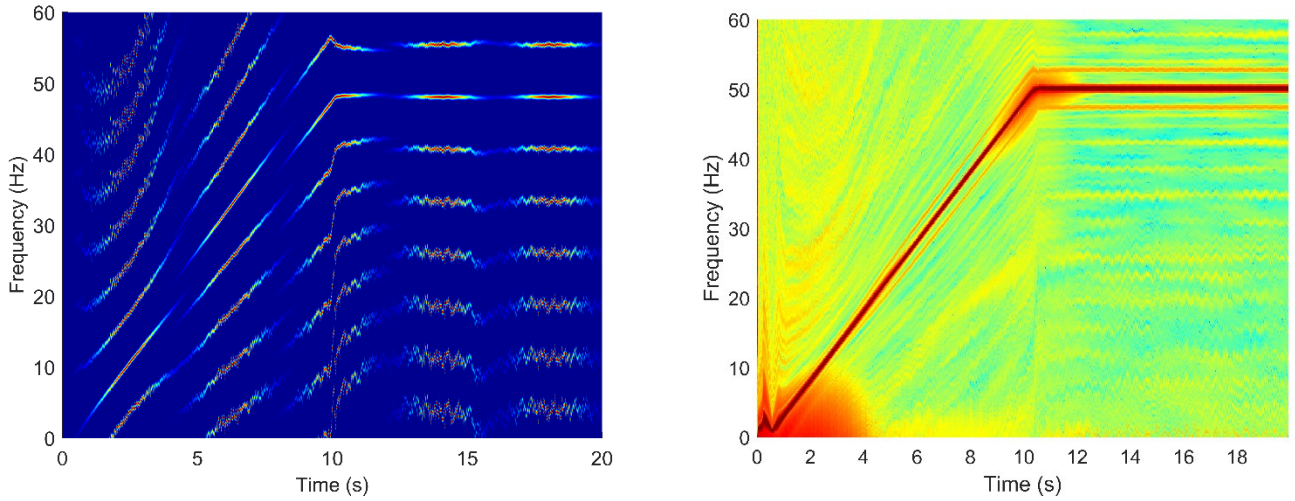

Fig. 8. Family of dragon atoms (left) and the resulting analysis (right) of the bar breakage motor current (Dragon Tansform).

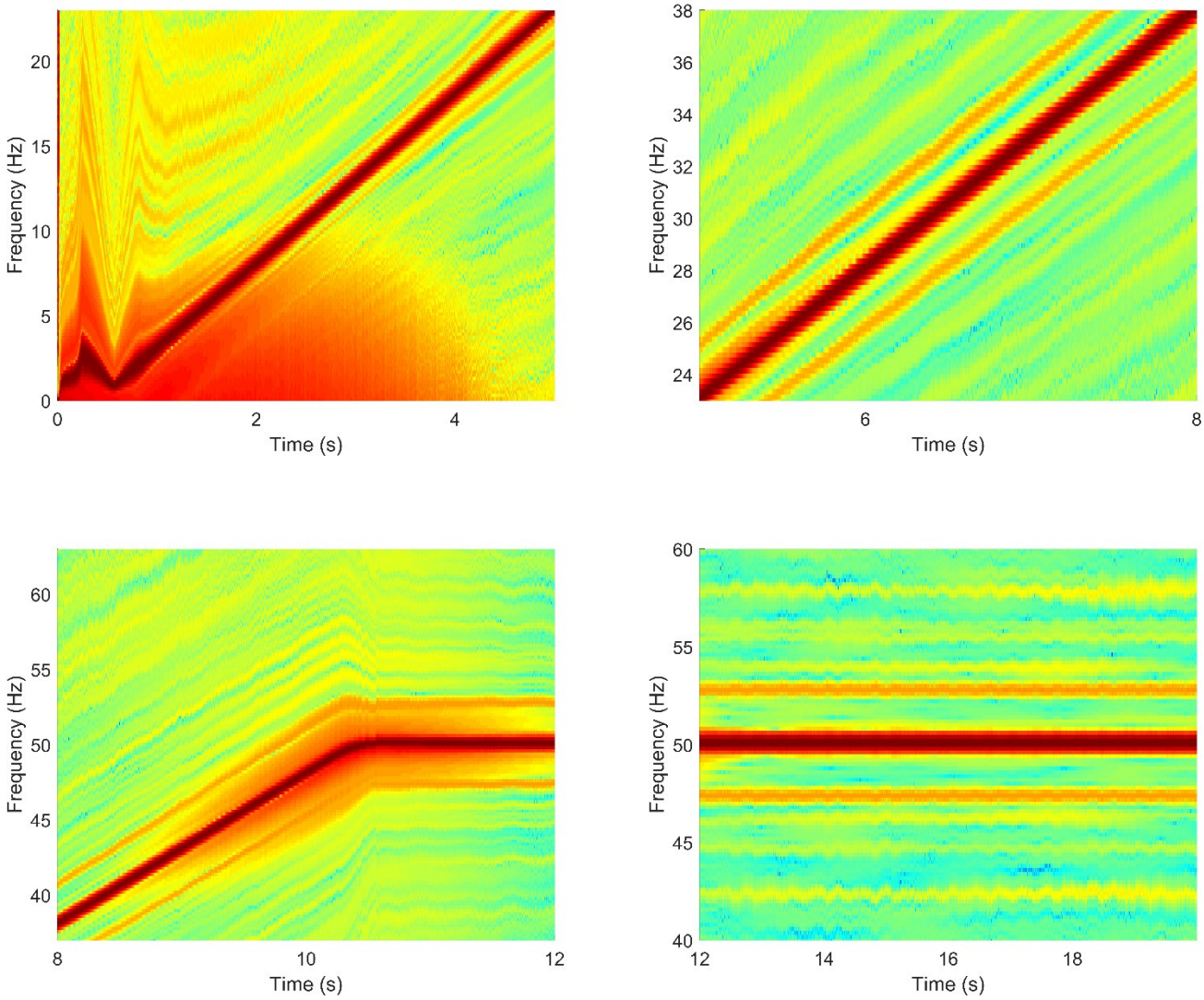

Fig. 9. Several zooms of the dragon transform result shown in Fig. 8 (right).

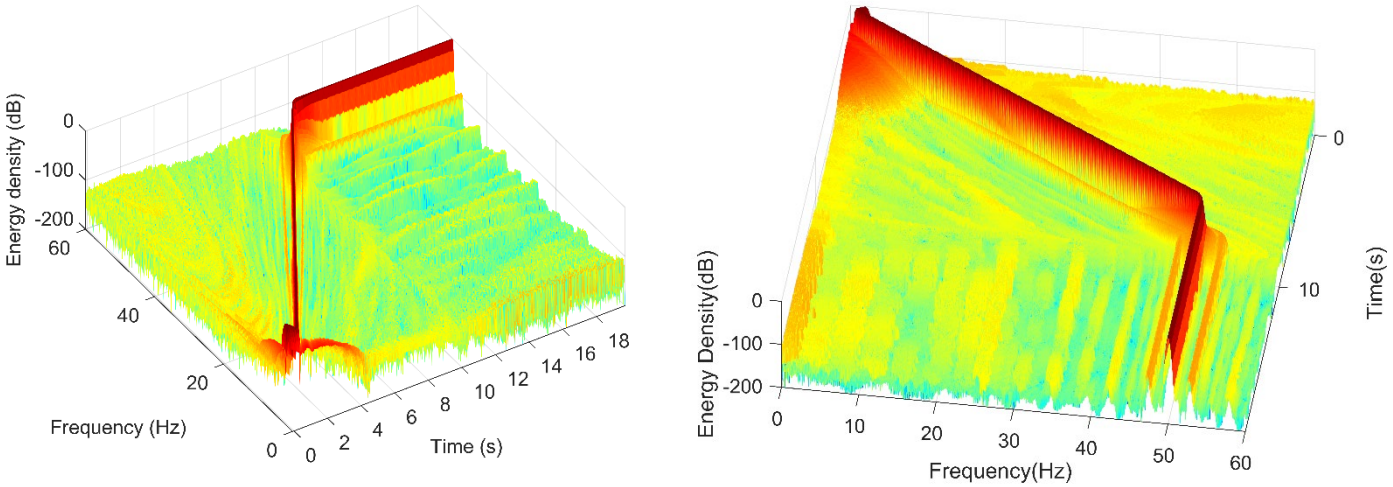

Fig. 10. 3D views of the dragon transform result when applied to the bar breakage motor current (Fig. 8, right).

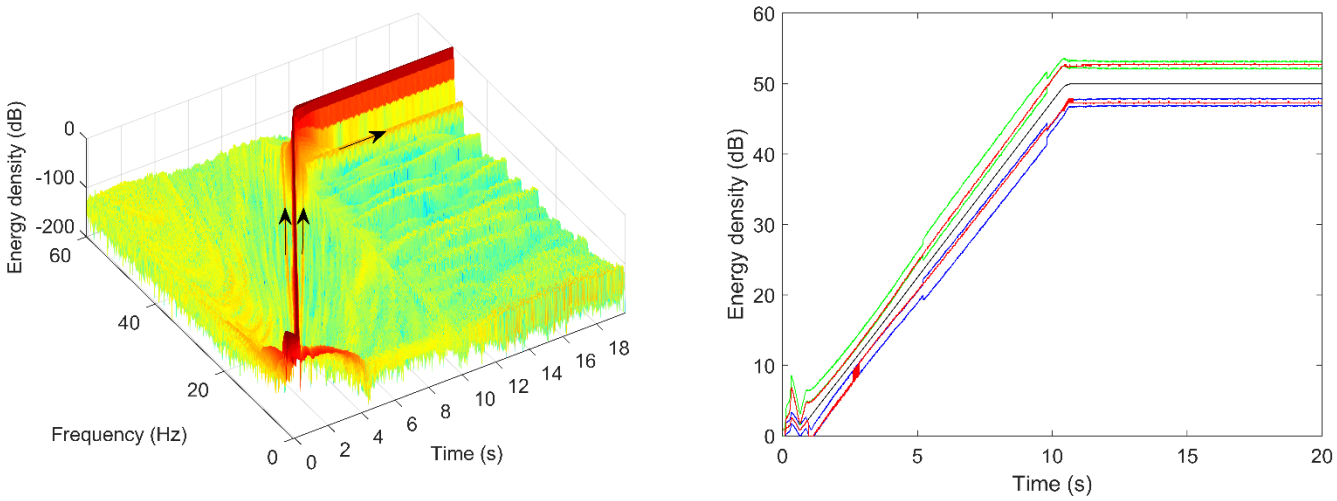

Fig. 21. 3D view of the dragon transform result when applied to the bar breakage motor current (Fig. 10, left) with the faulty harmonics evolutions marked with arrows (left). The FC evolution (black), the frequency bands along the faulty harmonics theoretical evolutions (green and blue), and the final bar breakage harmonic evolutions (red) (right).

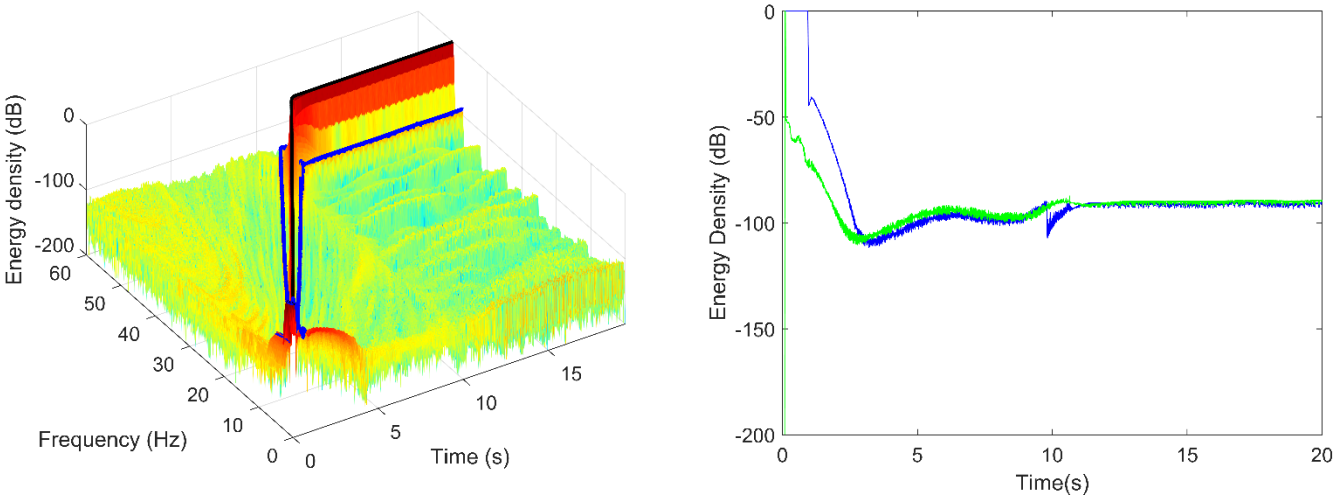

Fig. 12. 3D view of the dragon transform result when applied to the bar breakage motor current (Fig. 10, left) with the final bar breakage harmonic evolutions traced in blue and the FC evolution traced in black (left). The time evolution of the energy density along the bar breakage harmonics evolutions (blue and green) (right).

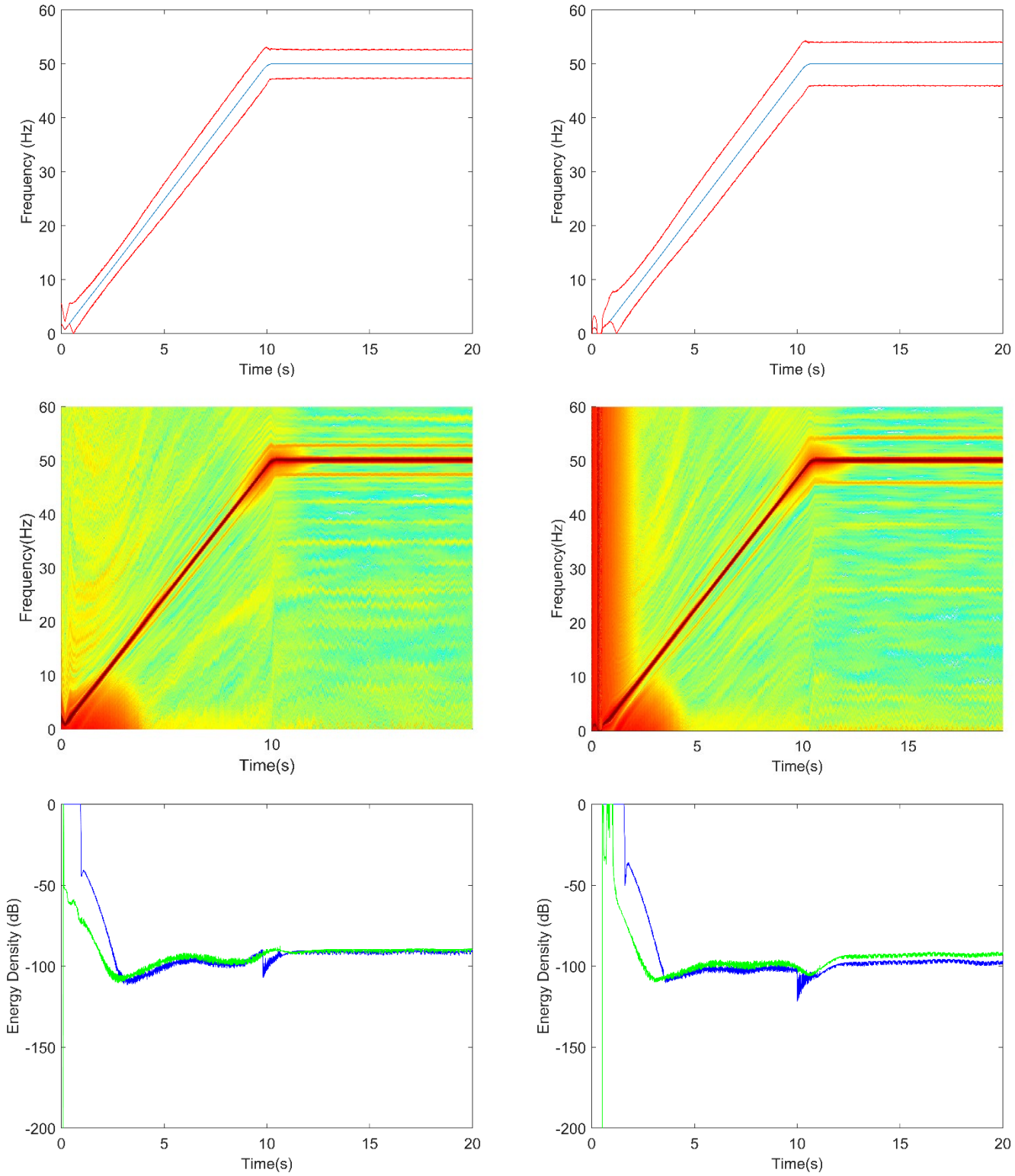

Fig. 3. Results for the bar breakage motor current under low load (left) and high load (right): evolution (top) of the FC (blue) and bar breakage harmonics (red), dragon transform (middle) and quantification (down).

References

[1] J. Tolvanen, Saving energy with variable speed drives, World Pumps, (501) (2008) 32-33.

[2] C. M. F. S. Reza, M. D. Islam, and S. Mekhilef, A review of reliable and energy efficient direct torque controlled induction motor drives, Renew. Sustain. Energy Rev., 37 (2014) 919-932.

[3] B. Payne, A. Ball and F. Gu, Detection and diagnosis of induction motor faults using statistical measures, International Journal of COMADEM, 5 (2002) 5-19.

[4] M. Akar, Detection of Rotor Bar Faults in Field Oriented Controlled Induction Motors, Journal of Power Electronics, 12 (2012) 982-991.

[5] L. Beneduce, G. Caruso, D. Iannuzzi, F. Maceri, E. Pagano and L. Piegari, Analysis of a structural failure mode arising in cage rotors of induction machines, Electrical Engineering, 93 (2011) 179-191.

[6] C. Bruzzese, O. Honorati and E. Santini, Rotor bars breakage in railway traction squirrel cage induction motors and diagnosis by MCSA technique part I : Accurate fault simulations and spectral analyses, in: Diagnostics for Electric Machines, Power Electronics and Drives, 2005. SDEMPED 2005. 5th IEEE International Symposium on, 2005, pp. 1-6.

[7] S. Nandi, H. A. Toliyat and Xiaodong Li, Condition monitoring and fault diagnosis of electrical motors-a review, IEEE Trans. Energy Conversion, 20 (2005) 719-729.

[8] J. Pons-Llinares, D. Morinigo-Sotelo, O. Duque-Perez, J. Antonino-Daviu, and M. Perez-Alonso, Transient detection of close components through the chirplet transform: Rotor faults in inverter-fed induction motors, in: Proc. 40th Annu. Conf. IEEE Ind. Electron. Soc. (IECON), 2014, pp. 3386-3392.

[9] D. Mills, M. A. Al-Tai and S. B. Tennakoon, Maintenance of AC traction motor on the modern UK railway network, in: Universities Power Engineering Conference, 2007. UPEC 2007. 42nd International, 2007, pp. 170-173.

[10] W. T. Thomson and M. Fenger, Current signature analysis to detect induction motor faults, IEEE Industry Applications Magazine, 7 (2001) 26-34.

[11] A. Bellini, F. Filippetti, C. Tassoni and G. -. Capolino, Advances in Diagnostic Techniques for Induction Machines, IEEE Transactions on Industrial Electronics, 55 (2008) 4109-4126.

[12] B. Sauer, H. Böhm and E. Scharstein, Squirrel cage rotor for an electrical motor., Germany Patent WO/1994/001918, 1993.

[13] G. Dressel, Electric machine with a squirrel-cage rotor, U.S. Patent 7215056, 2007.

[14] J. P. Amezquita-Sanchez, M. Valtierra-Rodriguez, D. Camarena-Martinez, D. Granados-Lieberman, R. J. Romero-Troncoso, and A. Dominguez-Gonzalez, Fractal dimension-based approach for detection of multiple combined faults on induction motors, J. Vibrat. Control, 22 (17) (2015) 3638-3648.

[15] J. Pons-Llinares, V. Climente-Alarcon, F. Vedreno-Santos, J. Antonino-Daviu and M. Riera-Guasp, Electric machines diagnosis techniques via transient current analysis, in: IECON 2012 - 38th Annual Conference on IEEE Industrial Electronics Society, 2012, pp. 3893-3900.

[16] V. Ghorbanian and J. Faiz, A survey on time and frequency characteristics of induction motors with broken rotor bars in line-start and inverter-fed modes, Mech. Syst. Signal Process., 54-55 (2015) 427-456.

[17] D. Morinigo-Sotelo, L. A. Garcia-Escudero, O. Duque-Perez, and M. Perez-Alonso, Practical aspects of mixed-eccentricity detection in PWM voltage-source-inverter-fed induction motors, IEEE Trans. Ind. Electron., 57 (1) (2010) 252-262.

[18] W. S. Abu-Elhaija, V. Ghorbanian, J. Faiz, and B. M. Ebrahimi, Impact of closed-loop control on behavior of inverter-fed induction motors with rotor broken-bars fault, in: Proc. IEEE Int. Conf. Power Electron., Drives Energy Syst. (PEDES), 2012, pp. 1-4.

[19] J. Faiz, V. Ghorbanian, and B. M. Ebrahimi, A survey on condition monitoring and fault diagnosis in line-start and inverter-fed broken bar induction motors, in: Proc. IEEE Int. Conf. Power Electron., Drives Energy Syst. (PEDES), 2012, pp. 1-5.

[20] J. Pons-Llinares, J. Antonino-Daviu, J. Roger-Folch, D. Morinigo-Sotelo and O. Duque-Perez, Eccentricity diagnosis in inverter - fed induction motors via the analytic wavelet transform of transient currents, in: Electrical Machines (ICEM), 2010 XIX International Conference on, 2010, pp. 1-6.

[21] T. M. Wolbank, G. Stojicic and P. Nussbaumer, Monitoring of partially broken rotor bars in induction machine drives, in: IECON 2010 - 36th Annual Conference on IEEE Industrial Electronics Society, 2010, pp. 912-917.

[22] J. R. Millan-Almaraza, R. J. Romero-Troncoso, R. A. Osornio-Rios and A. Garcia-Perez, Wavelet-based Methodology for Broken Bar Detection in Induction Motors with Variable-speed Drive, Electric Power Components and Systems, 39 (2011) 271-287.

[23] V. Fernandez-Cavero, D. Morinigo-Sotelo, O. Duque-Perez, and J. Pons-Llinares, A comparison of techniques for fault detection in inverter-fed induction motors in transient regime, IEEE Access, 5 (2017) 8048-8063.

[24] K. Teotrakool, M. J. Devaney, and L. Eren, Adjustable-speed drive bearing-fault detection via wavelet packet decomposition, IEEE Trans. Instrum. Meas., 58 (8) (2009) 2747-2754.

[25] M. Dlamini, P. S. Barendse, and A. M. Khan, Detecting faults in inverterfed induction motors during startup transient conditions, in: Proc. IEEE Energy Convers. Congr. Expo., 2014, pp. 3131-3138.

[26] J. Pons-Llinares, M. Riera-Guasp, J. A. Antonino-Daviu, and T. G. Habetler, Pursuing optimal electric machines transient diagnosis: The adaptive slope transform, Mech. Syst. Signal Process., 80 (2016) 553-569.

[27] J. Pons-Llinares, J. Antonino-Daviu, J. Roger-Folch, D. Moríñigo-Sotelo, O. Duque-Pérez, Mixed eccentricity diagnosis in Inverter-Fed Induction Motors via the Adaptive Slope Transform of transient stator currents, Mech. Syst. Signal Process., 48 (1–2) (2014) 423-435.

[28] S. Mann and S. Haykin, The Chirplet transform: A generalization of Gabor's logon transform, in: Proc. Vision Interface, 1991, pp. 205–212.

[29] T. A. Garcia-Calva, D. Morinigo-Sotelo, and R. de Jesus Romero-Troncoso, Non-uniform time resampling for diagnosing broken rotor bars in inverter-fed induction motors, IEEE Trans. Ind. Electron., 64 (3) (2017) 2306-2315.

[30] J. M. Aller, T. G. Habetler, R. G. Harley, R. M. Tallam, S. B. Lee, Sensorless speed measurement of ac machines using analytic wavelet transform, IEEE Trans. Ind. Appl., 38 (5) (2002) 1344–1350.

Vanessa Fernandez-Cavero received the B.S. degree in industrial organization engineering and electrical engineering from ICAI, Comillas Ponti_cal University, Madrid, Spain, in 2005.She is currently pursuing the Ph.D. degree with the University of Valladolid, Spain. Her current research interests include the monitoring of induction machines and the detection and diagnosis of faults in inverter-fed IM in transient regimes.

Joan Pons-Llinares received the M.Sc. degree in Industrial Engineering and the Ph.D. degree in Electrical Engineering from the Universitat Politècnica de València (UPV, Spain), in 2007 and 2013, respectively. He is currently an Assistant Professor in the Electric Engineering Department of the UPV. His research interests include time-frequency transforms, condition monitoring and diagnostics of electrical machines.

Daniel Morinigo-Sotelo received the B.S. and Ph.D. degrees in electrical engineering from the University of Valladolid (UVA), Spain, in 1999 and 2006, respectively. He was a Research Collaborator on Electromagnetic Processing of Materials with the Light Alloys Division of CIDAUT Foundation since 2000 until 2015. He is currently with the Research Group in Predictive Maintenance and Testing of Electrical Machines, Department of Electrical Engineering, UVA, and with the HSPdigital Research Group, Mexico. His current research interests include the condition monitoring of induction machines, optimal electromagnetic design, and heuristic optimization.

Oscar Duque-Perez received the B.S. and Ph.D. degrees in electrical engineering from the University of Valladolid (UVA), Spain, in 1992 and 2000, respectively. In 1994, he joined the E.T.S. de Ingenieros Industriales, UVA, where he is currently a Full Professor with the Research Group in Predictive Maintenance and Testing of Electrical Machines, Department of Electrical Engineering. His main research interests include power systems reliability, condition monitoring, and heuristic optimization techniques.